Energy loss of MeV protons specularly reflected from metal surfaces

J. I. Juaristi
Departamento Física de Materiales, Facultad de Químicas, Universidad del Pais Vasco/Euskal Herriko Unibersitatea, Apartado Postal 1072, 20080 San Sebastián, Spain

F. J. García de Abajo
Departamento Ciencias de la Computación e Inteligencia Artificial, Facultad de Informática, Universidad del Pais Vasco/Euskal Herriko Unibersitatea, Apartado Postal 649, 20080 San Sebastián, Spain

P. M. Echenique
Departamento Física de Materiales, Facultad de Químicas, Universidad del Pais Vasco/Euskal Herriko Unibersitatea, Apartado Postal 1072, 20080 San Sebastián, Spain

(Received 25 September 1995; revised manuscript received 15 December 1995)

A parameter-free model is presented to study the energy loss of fast protons specularly reflected from metal surfaces. The contributions to the energy loss from excitation of valence-band electrons and ionization of localized target-atom electronic states are calculated separately. The former is calculated from the induced surface wake potential using linear response theory and the specular-reflection model, while the latter is calculated in the first Born approximation. The results obtained are in good agreement with available experimental data. However, the experimental qualitative trend of the energy loss as a function of the angle of incidence is obtained when the valence-band electron model is replaced by localized target atom electron states, though with a worse quantitative agreement. [S0163-1829(96)07020-8]

I. INTRODUCTION

When an ion approaches a metal surface, the energy associated to its motion perpendicular to the surface determines whether it will penetrate the solid or will be reflected at the topmost atomic layer. If one wants to obtain information about the structure of the surface, one is interested in those trajectories for which the particle interacts with the metal surface for a long time before it is reflected. This situation is achieved by using projectiles with small energy in the normal motion, as is the case in grazing ion-surface collisions.

When the charged particle interacts with the surface, different processes may take place depending on its velocity relative to the velocity of the electrons in the metal. For ion velocities smaller[1–4] than or of the same order[5–7] as the velocity of the electrons of the metal conduction band ($\approx v_0$, the Bohr velocity, for typical metals), a complicated picture emerges in which the energy loss of the ion and charge transfer between metal and particle are interrelated. Charge transfer occurs mainly via resonant and Auger processes[8–10] and the energy lost by the charge goes to creation of excitations in the valence band of the solid.

For high projectile velocities ($v \gg v_0$) the charge state is fixed, and the particle may induce inner-shell excitations in the target atoms, as well as valence-band excitations.[11–13]

In this paper, we present a parameter-free theoretical study of the energy loss of protons grazingly incident over metal surfaces in the fast velocity regime ($v > 4v_0$). We will consider trajectories such that the projectiles are reflected in front of the first atomic layer. For the velocities under consideration, this implies that we have to deal with angles of incidence φ of the order of mrad. This geometry is adequate to analyze metal surfaces because it results in a long interaction time between the particle and the target. Moreover, we shall assume, as a plausible approximation valid for high velocities, that the protons stay bare along their entire trajectory. Possible electronic excitations of the surface will be modeled.

The organization of this paper is as follows: in Sec. II the theoretical model is introduced; the results for an aluminum surface together with results and a comparison with available experimental data for PbSe and SnTe are presented in Sec. III; the main conclusions are summarized in Sec. IV. Atomic units (a.u.) will be used unless stated otherwise.

II. THEORETICAL MODEL

In the study of the energy loss of a charged particle incident on a metal surface, we face the problem related to the different regions that the particle feels during its trajectory. Knowing the exact trajectory, i.e., the position of the particle at any time t, and the energy loss per unit time dE/dt at any point of the trajectory, one can calculate the total energy loss performing the following integral:

$$\Delta E = \int_{-\infty}^{\infty} \frac{dE}{dt}\, dt. \tag{1}$$

In this work, we shall focus on the energy loss of MeV protons moving with small glancing angles of incidence of the order of mrad. This geometry is particularly simple from the theoretical point of view for several reasons. No relevant charge transfer should be expected to occur between metal and proton at such high velocities, $v > 4$ a.u. Besides, the small angles of incidence make the proton-position coordi-

nate perpendicular to the surface, z, a slowly varying function of time, as compared with the motion along the direction parallel to the surface. This permits us to calculate the energy loss per unit time in an idealized parallel trajectory and to obtain the energy loss by integrating over z, the impact parameter of such a trajectory, i.e., we change variable t by z in the integral of Eq. (1) and calculate dE/dt for a parallel trajectory. We will consider that the trajectory is parallel to a random direction of the surface, so that there are no channeling effects.[14] Moreover, the ions are assumed to be specularly reflected on the surface, thus, the incoming and outgoing trajectories are identical and it is enough to carry out the calculation only in the outgoing part. Consequently, the total energy loss takes the form

$$\Delta E = 2\int_{z_0}^{\infty} \frac{dE}{dt}(z)\,\frac{1}{v_z(z)}\,dz, \tag{2}$$

where z_0 is the distance of closest approach at the turning point, and v_z is the component of the velocity perpendicular to the surface.

This integral involves the product of two quantities that one needs to calculate. The first one is $dE/dt(z)$, i.e., the energy loss per unit time for a proton traveling parallel to the surface at a distance z from the first atomic plane. This magnitude is related to the different excitations that the projectile may induce in the metal target.

The second magnitude is the normal velocity $v_z(z)$. The important point concerning this magnitude is that its value actually does change along the trajectory. At distances far from the surface, v_z goes to $v_z = v \sin(\varphi)$, where v is the velocity of the proton, which we assume to be constant during all of the interaction time, due to the fact that the energy loss is much smaller than the projectile energy. In the incoming part of the trajectory, when the proton gets closer to the surface, the attractive image potential accelerates it towards the surface and the value of v_z increases. Finally, close to the turning point the repulsive atomic potential decelerates the proton and v_z goes to zero as z approaches z_0. These considerations must be taken into account and their effect will be discussed below.

A. Calculation of dE/dt

When the proton interacts with the metal surface, it induces electronic excitations in the medium, and therefore, it loses energy. We distinguish here between two different contributions to the energy loss or, in other words, we separate the electrons of the solid into two different groups according to their binding energy.

We calculate separately the energy loss per unit time due to (1) the excitation of valence-band electrons, dE_{val}/dt, and (2) the excitation of electron bound states of the target atoms, i.e., inner-shell excitations, dE_s/dt.

The total energy loss per unit time is the sum of both contributions:

$$\frac{dE}{dt} = \frac{dE_{\mathrm{val}}}{dt} + \frac{dE_s}{dt}. \tag{3}$$

This quantity depends on the distance of the ion from the surface (first atomic layer) z.

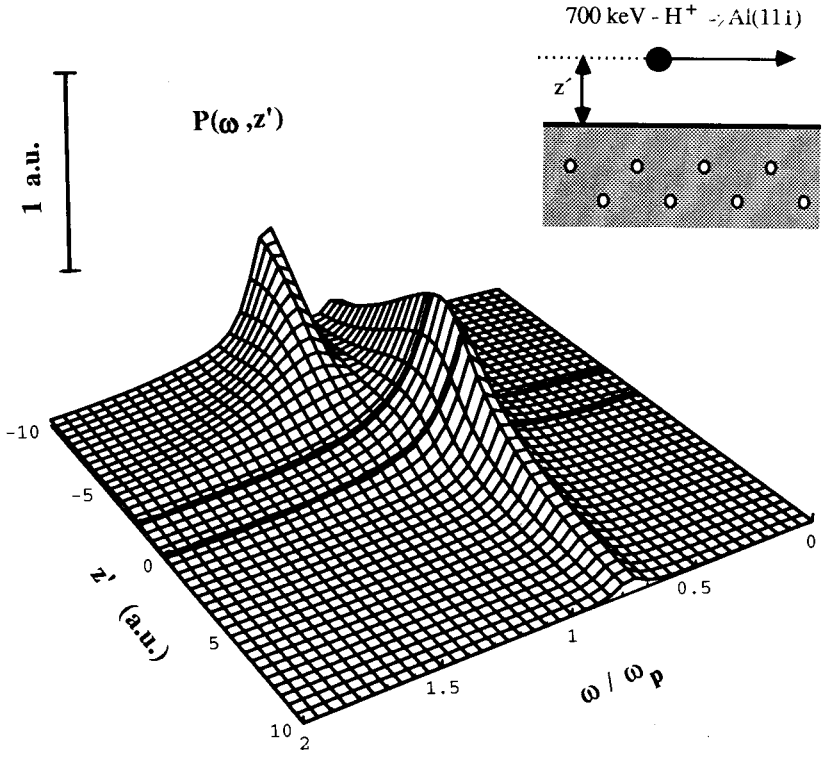

FIG. 1. Probability of creating an excitation of energy ω when a 700-keV proton is traveling parallel to an aluminum surface at a distance z' with respect to the jellium edge calculated according to Eq. (7). The position of the jellium edge and the topmost atomic layer are shown by thick-curves. In this figure, $\omega_p = 15.8$ eV is the classical plasmon frequency that corresponds to $r_s = 2.07$ a.u. The value of the damping is $\gamma = 1.35$ eV.

1. Excitation of valence-band electrons

In this contribution, we include the excitation of both collective modes and single particles of the valence band of the solid, for which we assume a jellium model of independent electron states bounded by a surface barrier potential. For a proton moving along a direction x parallel to a surface, the energy loss is calculated in terms of the force due to the induced surface wake potential $\phi_{\rm ind}$:[15,16]

$$\frac{dE_{\rm val}}{dt}(z')=v\,\frac{\partial\phi_{\rm ind}}{\partial x}(z'), \tag{4}$$

where z' is the separation between the proton and the jellium edge (or electronic surface). Concerning the location of the electronic surface, we will use the standard prescription, which consists in placing it at a distance $d/2$ in front of the first atomic layer, where d is the interplanar separation, i.e., $z'=z-d/2$. The derivative of Eq. (4) is evaluated at the position of the proton, that is,

$$\frac{\partial\phi_{\rm ind}}{\partial x}(z')=\frac{\partial\phi_{\rm ind}}{\partial x}(\mathbf{r},t);\quad \mathbf{r}=(vt,0,z'). \tag{5}$$

The surface wake potential is calculated here using the specular-reflection model,[17,18] which allows one to express the response of the surface in terms of the dielectric function of the bulk material $\epsilon(k,\omega)$. In this way, nonlocal effects are introduced through dispersion in the latter. This model relies on the assumption that the surface potential barrier is infinite for the valence electrons. Moreover, the quantum interference between outgoing and reflected components of the wave functions of solid electrons is neglected. The specular-reflection model has been widely applied to ion-surface interaction related problems[19,20] and it is expected to work well for the large velocities under consideration.

In this way expression (4) can be written as follows:[21,22]

$$\frac{dE_{\rm val}}{dt}(z')=\int_0^\infty d\omega\ \omega P(\omega,z'). \tag{6}$$

where $P(\omega,z')$ is the probability per unit time that a proton traveling parallel to the electronic surface at a distance z' creates an excitation of energy ω. More precisely,[23,24]

$$P(\omega,z')=\begin{cases} -\dfrac{2}{\pi v}\displaystyle\int_0^\infty\frac{dq}{Q}\,{\rm Im}\left\{\frac{\epsilon_s(Q,\omega)-1}{\epsilon_s(Q,\omega)+1}\right\}\exp(-2Qz'),\quad z'>0, & \text{(7a)}\\ -\dfrac{2}{\pi v}\displaystyle\int_0^\infty\frac{dq}{Q}\,{\rm Im}\left\{\epsilon_s(Q,\omega)+\epsilon_s(Q,2z',\omega)-\frac{2(\epsilon_s(Q,z',\omega))^2}{\epsilon_s(Q,\omega)+1}\right\},\quad z'<0, & \text{(7b)}\end{cases}$$

where $Q=\sqrt{q^2+\omega^2/v^2}$, $\epsilon_s(Q,z',\omega)$ is calculated according to the expression:

$$\epsilon_s(Q,z',\omega)=\frac{Q}{\pi}\int_{-\infty}^{\infty}\frac{dk_z}{k^2}\frac{\exp(ik_zz')}{\epsilon(k,\omega)}, \tag{8}$$

$\epsilon_s(Q,\omega)=\epsilon_s(Q,0,\omega)$, $k^2=k_z^2+Q^2$, and $\epsilon(k,\omega)$ is the bulk response function, for which the random-phase approximation[25] (RPA) will be used, together with the Mermin prescription,[26] which permits us to incorporate a finite damping (γ) to the electron motion while keeping the number of electrons in the system constant.

Figure 1 shows the different contributions to the loss, $P(\omega,z')$, for different values of ω. Notice that the surface modes are dominant near the electronic surface, while bulk plasmons appear well below the surface. This is a manifestation of the so-called begrenzung effect,[15] consisting in the inhibition of bulk modes in favor of surface modes in the subsurface region of the material. This effect has been observed clearly using scanning transmission electron microscopy techniques.[27,28,22] The main contribution to the losses for a grazing trajectory comes from the excitation of surface plasmons of frequency slightly larger than the classical surface plasmon frequency ω_s. This is due to the effect of dispersion on the surface modes, which is positive in the specular-reflection model.

2. Excitation of inner shells of target atoms

We call inner-shell electrons those electrons of the solid that are not in the valence band. For the high velocities under consideration, the contribution of these electrons to the stopping can be quite large. The inner-shell electrons are strongly localized around target atoms, and therefore, for a trajectory such that the projectiles do not penetrate beyond the topmost atomic layer, only electrons of atoms located at the first atomic plane can be effectively excited by the projectile, and consequently, these electrons are the only inner-shell electrons that contribute to the proton energy loss.

In this work, the energy loss originating in the interaction of a proton with the first layer of target atoms is expressed in terms of the impact-parameter-dependent energy loss in single encounters of the proton with target atoms P. An average over the trajectory is performed. One finds

$$\frac{dE_s}{dt}(z)=\frac{2v}{\Omega}\int_0^\infty dy\ P(\sqrt{y^2+z^2}), \tag{9}$$

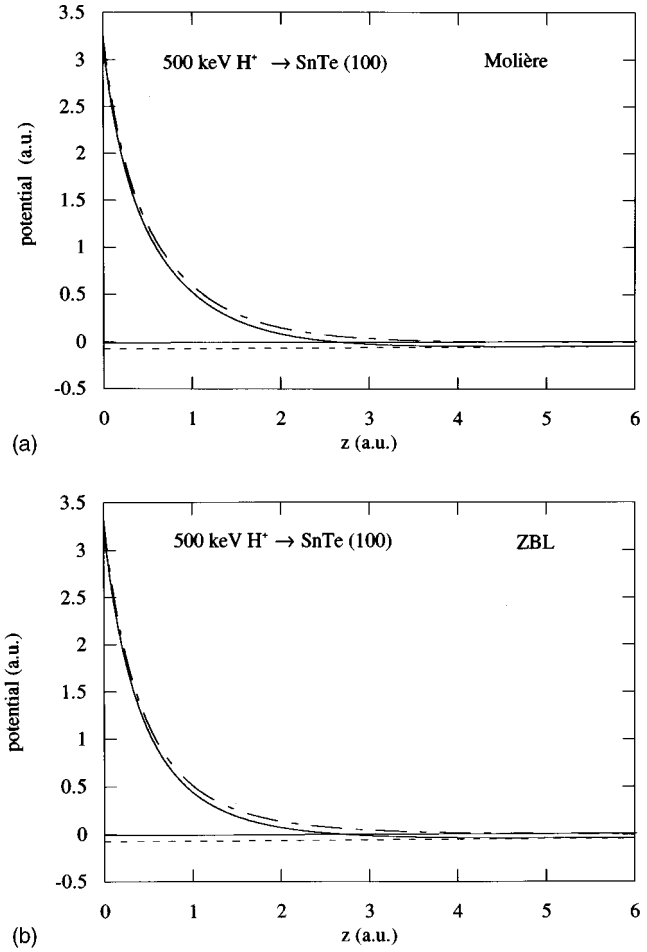

FIG. 2. (a) Interaction potential between a 500-keV proton and a SnTe(100) surface as a function of the distance to the first atomic layer. The dashed line corresponds to the attractive ϕ^I image potential. The electron gas parameters are $r_s=2.14$ a.u. and $\gamma=5$ eV. The dashed-dotted line is the crystal potential $V(z)$ calculated in the Molière approximation. The solid line represents the total potential $U(z)$. (b) The same as (a), using the ZBL approximation rather than the Molière potential.

where y is the coordinate directed parallel to the surface and perpendicular to the velocity, and Ω is the area per target atom in the first atomic layer.

The energy loss P is taken as due to ionization of the target atoms. Thus, it is calculated summing the energy loss originating in the ionization from all different occupied inner-shell electron states P_i. It reads

$$P(b)=\sum_i P_i(b), \tag{10}$$

where the index i runs over all occupied inner-shell electron states and b is the impact parameter of the collision. In practice, it is not necessary to perform the calculation of P_i for all electrons, since those with average velocity much faster than the velocity of the projectile will produce a negligible contribution.

$P_i(b)$ can be calculated using the following expression:

$$P_i(b)=\int_0^\infty (\epsilon+\epsilon_i)\omega_i(\epsilon,b)d\epsilon, \tag{11}$$

where $\omega_i(\epsilon,b)$ is the probability for ionizing an electron from an initial bound state i with ionization potential ϵ_i to the final free state corresponding to an energy ϵ, in a collision with impact parameter b. This magnitude can be calculated in terms of $a_{if}(\mathbf{b},\epsilon)$, that is, the amplitude for the transition from the bound state i to the state of the continuum f of energy ϵ and well-defined angular momentum, as a function of the impact parameter vector $\mathbf{b}$:

$$\omega_i(\epsilon,b)=\sum_f \omega_{if}(\epsilon,b), \tag{12}$$

$$\omega_{if}(\epsilon,b)=\frac{1}{2\pi}\int_0^{2\pi} d\varphi |a_{if}(\mathbf{b},\epsilon)|^2, \tag{13}$$

where the summation in Eq. (12) runs over all states f with the same energy ϵ, and the integral in expression (13) is carried out over φ the azimuthal angle of $\mathbf{b}$. The amplitude $a_{if}(\mathbf{b},\epsilon)$ depends on the direction of $\mathbf{b}$ through the relative orientation of the states. Expression (13) corresponds to the average of $a_{if}(\mathbf{b},\epsilon)$ over all different orientations. If our system had azimuthal symmetry (in general this is not the case), $\omega_{if}(\epsilon,b)$ would reduce to

$$\omega_{if}(\epsilon,b)=|a_{if}(b,\epsilon)|^2. \tag{14}$$

In the first Born approximation, $a_{if}(\mathbf{b},\epsilon)$ reads[29,30]

$$a_{if}(\mathbf{b},\epsilon)=\frac{1}{4\pi^2 v}\int d\boldsymbol{\eta}\, \exp(i\boldsymbol{\eta}\cdot\mathbf{b})T_{if}(\boldsymbol{\eta},\epsilon), \tag{15}$$

where

$$T_{if}(\boldsymbol{\eta},\epsilon)=\frac{4\pi}{q^2}\langle f|\exp(i\mathbf{q}\cdot\mathbf{r})|i\rangle, \tag{16}$$

v is the velocity of the proton, $\mathbf{r}$ is the electron position coordinate relative to the target atom, and $\mathbf{q}$ is the momentum transferred in the interaction, which can be separated into longitudinal and transverse components:

$$\mathbf{q}=\mathbf{q}_\parallel+\boldsymbol{\eta}=\frac{\Delta E}{v}\hat{v}+\boldsymbol{\eta}, \quad \boldsymbol{\eta}\cdot\hat{v}=0, \tag{17}$$

and ΔE is the total energy transferred to the electron:

$$\Delta E=\epsilon+\epsilon_i. \tag{18}$$

The energy of the atomic levels and their wave functions are approximated by the values calculated for neutral atoms. No correction is included to take into account that the atoms are not isolated and that they are part of a metal surface. Therefore, for the description of the target atom states, we have used a model approach based on the Hartree-Fock-Slater (HFS) potential calculated from the program of Desclaux.[31] The electronic states and their wave functions are determined numerically with the Numerov algorithm as eigenstates of the one-electron Hamiltonian using the HFS potential. This approach is not only valid for the calculation of the occupied fundamental state wave functions but also for the final states of the continuum that have to be consid-

ered in the ionization process, since our calculations depend on the part of the wave functions of the continuum that overlaps strongly with the localized bound orbitals, i.e., the region close to the ion core.[32]

B. Calculation of the trajectory: $v_z(z)$

The component of the velocity normal to the surface v_z can be expressed, assuming conservation of energy in the perpendicular direction, in the form

$$\tfrac{1}{2}M(v\ \sin\varphi)^2=\tfrac{1}{2}Mv_z^2+U(z). \tag{19}$$

In the above expression, M is the mass of the proton and $U(z)$ is the interaction potential between proton and surface. Two different contributions can be distinguished in the potential $U(z)$. The repulsive static crystal potential $V(z)$, originating in the interaction with target atoms, and the attractive image potential $\phi^I(z)$, which is obtained using the same approximation[23,24] as in Eqs. (7) and (8):

$$U(z)=V(z)+\phi^I(z). \tag{20}$$

The image potential is calculated as

$$\phi^I(z)=\begin{cases}\dfrac{1}{\pi v}\displaystyle\int_0^\infty d\omega\int_0^\infty\frac{dq}{Q}\,\mathrm{Re}\left\{\frac{\epsilon_s(Q,\omega)-1}{\epsilon_s(Q,\omega)+1}\right\}\exp(-2Qz'), & z'>0 \quad (21a)\\[2ex] \dfrac{1}{\pi v}\displaystyle\int_0^\infty d\omega\int_0^\infty\frac{dq}{Q}\,\mathrm{Re}\left\{\epsilon_s(Q,\omega)+\epsilon_s(Q,2z',\omega)-\frac{2[\epsilon_s(Q,z',\omega)]^2}{\epsilon_s(Q,\omega)+1}-1\right\}, & z'<0, \quad (21b)\end{cases}$$

where all quantities are defined as in Eqs. (7) and (8). The image potential is calculated as one-half of the induced potential. Recent experiments show[33] that the image potential acceleration should be included in a correct calculation of the trajectory.

The crystal potential is made up of the interaction with all atoms in the solid. A pair-potential picture will be applied here for the sake of simplicity. Two different approximations will be used throughout this work for the interatomic potential between the proton and a target atom of atomic number Z_T: the Molière potential[34] and the Ziegler-Biersack-Littmark (ZBL) potential.[35] In both cases the potential takes the following form:

$$A(r)=\frac{Z_T}{r}\sum_{i=1}^{n}\gamma_i\exp(-\beta_i r), \tag{22}$$

where for the Molière potential $n=3$, $\gamma_i=(0.35,0.55,0.1)$, $\beta_i=(0.3/a_{TF},1.2/a_{TF},6/a_{TF})$, and $a_{TF}=0.88534/(\sqrt{Z_T}+1)^{2/3}$, whereas for the ZBL potential $n=4$, $\gamma_i=(0.028171,0.28022,0.50986,0.18175)$, $\beta_i=(0.20162/a_u,0.40290/a_u,0.94229/a_u,3.1998/a_u,)$ and $a_u=0.88534/(Z_T^{0.23}+1)$. r is the distance between the proton and the target atom.

The potential created by one surface layer at the position of the proton, as a function of the proton-surface layer separation z, may be written as follows:

$$V^0(z)=\frac{2\pi}{\Omega}\int_0^\infty\rho\ d\rho A(\sqrt{\rho^2+z^2})$$

$$=\frac{2\pi}{\Omega}Z_T\sum_{i=1}^{n}\frac{\gamma_i}{\beta_i}\exp(-\beta_i z), \tag{23}$$

where $\rho=\sqrt{x^2+y^2}$, and x and y are the coordinates along the directions parallel to the layer. In our calculation, we approximate $V(z)$, the crystal potential, by the sum of the potentials created by the three outer atomic layers. This is a good approximation because $V^0(z)$ is a short-range potential, as can be inferred from the exponential decay with the distance that is reflected in Eq. (23).

In Fig. 2 we present the values of $\phi^I(z)$, $V(z)$, and the total interaction potential $U(z)$ for 500-keV protons incident on a SnTe(100) surface. In Fig. 2(a) $V(z)$ is calculated using the Molière approximation whereas in Fig. 2(b) it is calculated using the ZBL approximation. Close to the surface, $V(z)$ is much stronger than the image potential, and only far from the surface ($z>3$) the image potential is the dominant contribution. Therefore, the image potential produces a nonnegligible effect for trajectories with very small angle of incidence that do not get very close to the surface. This effect can be seen in Fig. 3 in which different trajectories calculated using our model potentials are presented. In this figure, results for 500-keV protons incident on SnTe(100) with two different angles of incidence ($\varphi=1$ and 6 mrad) obtained with and without including the image potential are shown. In the case of $\varphi=6$ mrad, the inclusion of the image potential does not change the trajectory significantly. On the contrary, for $\varphi=1$ mrad the image potential gives rise to a strong effect. There is not a strong difference between using the Molière and the ZBL potentials. In order to look into this interatomic potential dependence more carefully, Fig. 4 shows the difference between the ZBL and Molière potentials as a function of the distance to the atomic surface for protons incidents on a SnTe(100) surface. The difference is always smaller than 0.1 a.u.: thus, whichever approximation we use for the atomic potential we will expect to obtain similar results.

Expression (19) permits us to calculate the turning point of the trajectory z_0, i.e., the lowest limit of integration of Eq. (2). z_0 corresponds to the vanishing of v_z, thus from Eq. (19)

$$U(z_0)=\tfrac{1}{2}M(v\ \sin\varphi)^2. \tag{24}$$

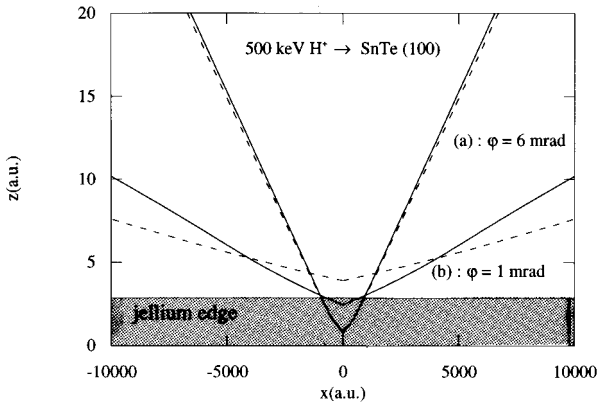

FIG. 3. Trajectories for 500-keV protons reflected on a SnTe(100) surface. The crystal potential has been calculated in the ZBL approximation. The (a) trajectories correspond to an angle of incidence φ=6 mrad, and (b) trajectories to an angle of incidence φ=1 mrad. The dashed lines correspond to trajectories calculated without including the image potential, and the solid lines stand for trajectories calculated including the image potential. We have taken r_s=2.14 a.u. and γ=5 eV.

Figure 5 represents z_0 calculated from Eq. (24) for 500-keV protons incident on a SnTe(100) surface as a function of the angle of incidence. Results obtained with the Molière and ZBL potentials including and neglecting the image potential are presented. The effect of including the image potential is again stronger for smaller angles of incidence. The change of the interatomic potential seems to have a weak effect.

III. RESULTS AND DISCUSSION

Next, we present results for protons incident on an Al(111) surface. An aluminum single neutral atom has 13 electrons organized in a $[\mathrm{Ne}]3s^2 3p^1$ electronic structure. The M-shell electrons give rise to the band structure of aluminum in its condensed phase. They are the so-called valence-band electrons, and their contribution to energy loss is calculated here using Eqs. (4)–(8). In this formalism we need to specify the electronic density of the conduction band, n, and the damping γ. For aluminum, we take r_s=2.07 a.u.

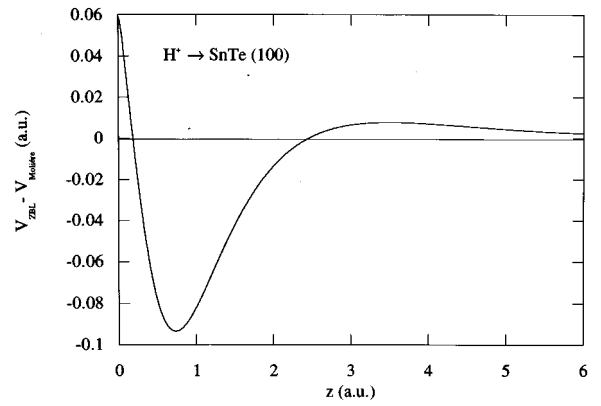

FIG. 4. Difference between the planar ZBL potential and the planar Molière potential ($V_{\mathrm{ZBL}}-V_{\mathrm{Molière}}$) acting on a proton near a SnTe(100) surface as a function of the distance of the proton to the first atomic layer.

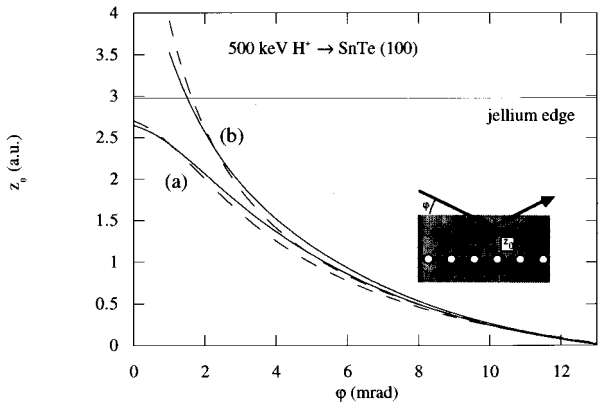

FIG. 5. Turning point of the trajectory of 500-keV protons incident on a SnTe(100) surface as a function of the angle of incidence. Curves a are obtained including the image potential and curves b without including it. The electron gas parameters are r_s=2.14 a.u. and γ=5 eV. The solid lines are obtained using the Molière potential to calculate the crystal potential, and the dashed lines with the ZBL potential.

and γ=1.35 eV, where $r_s=\sqrt[3]{3/4\pi n}$.

The inner-shell contribution to energy loss is obtained from the ionization of $2p$ and $2s$ states, since the contribution of the ionization of the $1s$ state is negligible in this range of energies.

A. Analysis of the contributions to the energy loss per unit time

In Fig. 6 we present our results for dE/dt in the case of 700-keV protons as a function of the distance from an aluminum (111) surface. We plot the different contributions to dE/dt and the total sum. It is important to stress the different

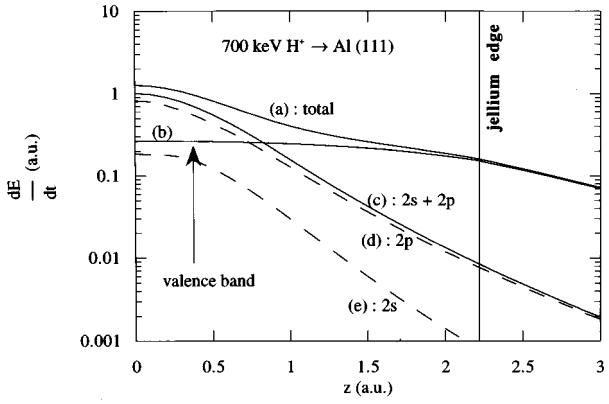

FIG. 6. Energy loss per unit time of 700-keV protons as a function of the distance from the first plane of atoms of an aluminum (111) surface. The solid curve a is the total dE/dt, sum of all other contributions, the solid curve b is the contribution due to excitation of valence-band electrons dE_{val}/dt and the solid curve c is the contribution of inner-shell excitations dE_s/dt. This last contribution is the sum of the energy loss per unit time originating in the ionization from the $2p$ orbital shown by the dashed curve d, and from the $2s$ orbital shown by the dashed curve e. In the description of the valence band of aluminum r_s=2.07 and γ=1.35 eV have been used.

behavior with the distance of the valence-band contribution $dE_{\rm val}/dt$ as compared to the inner-shell contribution dE_s/dt. dE_s/dt takes significant values at distances of the order of the target atoms size, where it dominates over $dE_{\rm val}/dt$ in the range of energies under consideration. On the other hand, the valence-band contribution is relevant at distances $z' \leq v/\omega_s$ (Refs. 36 and 37) with respect to the jellium edge, where ω_s is the classical surface plasmon frequency ($\omega_s=\omega_p/\sqrt{2}$), and it goes to a constant value inside the solid. Notice that the electronic surface is located at $z=d/2$ ($\approx$2.2 a.u. $\approx$1.17 Å for Al) outside the atomic surface, and therefore dE_s/dt is considerably smaller than $dE_{\rm val}/dt$ in that region. Consequently, $dE_{\rm val}/dt$ dominates over dE_s/dt except very close to the surface.

It has to be stated that the picture is completely different from that of a transmission experiment, where most of the energy loss occurs inside the solid so that bulk properties are analyzed instead of surface properties. More precisely, ionization of the L shell dominates over the losses against the conduction band in the bulk within this range of energies. Actually, the energy loss originating in the excitation of inner shells in the bulk is obtained averaging over impact parameters, and in the surface case there exists a selection of impact parameters.

The total energy loss per unit time dE/dt decreases with the distance rather rapidly (one order of magnitude in 3 a.u.). Moreover, the normal velocity of the particle v_z goes to zero near the turning point z_0. So that, since the integrand of Eq. (2), which gives us the total energy loss, is the product of dE/dt and $1/v_z$, the major contribution to that integral comes from the region close to z_0. In other words, the main contribution to the energy loss comes from the region close to the distance of closest approach, because, firstly, there the proton loses more energy per unit time (dE/dt gets its highest values) and, secondly, it travels for a longer time through this region (v_z is small).

Figure 7 is the same as Fig. 6 for 1.5-MeV incident protons. The results are similar in both cases. We find out that dE/dt is almost independent of the velocity. Notice, however, that $dE_{\rm val}/dt$ is larger at the surface in the case of 700-keV protons. This is related to the well-known $1/v^2$ dependence of the valence-band stopping power [$S=(1/v)dE/dt$] for large energies,[38] so that $dE_{\rm val}/dt$ goes as $1/v$. On the other hand, we observe that the decay of $dE_{\rm val}/dt$ with increasing distance to the surface is slower in the 1.5-MeV case, as a reflection of the linear behavior with the velocity of the characteristic range of the dynamic surface wake potential, v/ω_s.

B. Total energy loss

In Figs. 8 and 9 we show different contributions to the total energy loss ΔE as a function of the grazing angle of incidence φ for 700-keV and 1.5-MeV protons, respectively. The Molière potential has been used in the calculation of the trajectory. We find a completely different behavior of the valence-band contribution $\Delta E_{\rm val}$ and the inner-shell contribution ΔE_s. $\Delta E_{\rm val}$ decreases and ΔE_s increases with increasing angle of incidence. The reason for this can be easily understood from the dependence of both $dE_{\rm val}/dt$ and dE_s/dt on the distance to the surface (see Figs. 6 and 7) and the different proton trajectories for different angles of incidence (see Fig. 3). Increasing the angle of incidence results in the reduction of the time that the proton spends close to the surface, where $dE_{\rm val}/dt$ varies slowly with z. Consequently, the higher φ the smaller $\Delta E_{\rm val}$. Actually, for trajectories in which the proton crosses the jellium edge, the energy loss due to excitations of the valence band can be approximated by

$$\Delta E_{\rm val} \approx L \frac{dE_{\rm bulk}}{dx}, \tag{25}$$

where $dE_{\rm bulk}/dx$ is the stopping power in the bulk due to valence-band excitations, and L is the distance that the pro-

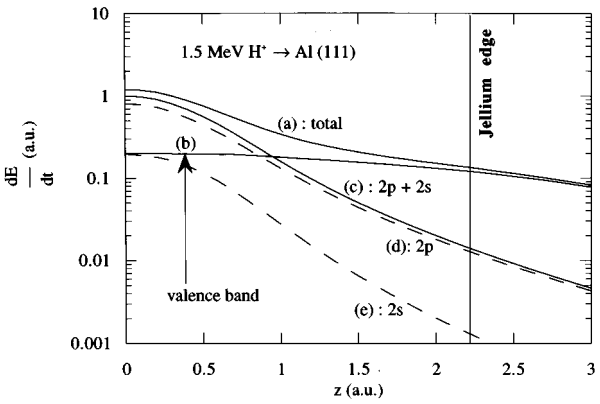

FIG. 7. Energy loss per unit time of 1.5-MeV protons as a function of the distance from the first plane of atoms of an aluminum (111) surface. The solid curve a is the total dE/dt sum of all other contributions, the solid curve b is the contribution due to excitation of valence-band electrons $dE_{\rm val}/dt$, the solid curve c is the contribution of inner-shell excitation dE_s/dt. This last contribution is the sum of the energy loss per unit time originating in the ionization from the $2p$ orbital shown by the dashed curve d, and in the ionization from the $2s$ orbital shown by the dashed curve e. In the description of the valence band of aluminum $r_s=2.07$ and $\gamma=1.35$ eV have been used.

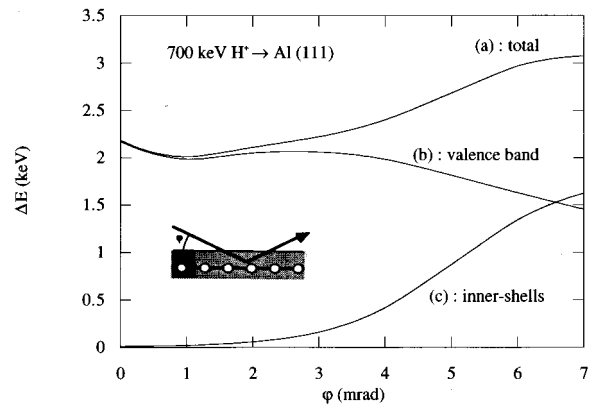

FIG. 8. Energy loss of 700-keV protons specularly reflected from an aluminum (111) surface as a function of the angle of incidence. Curve a is the total energy loss, curve b is the contribution of the valence-band excitations and curve c is the contribution of inner-shell excitations. In the description of the valence band of aluminum $r_s=2.07$ and $\gamma=1.35$ eV have been used.

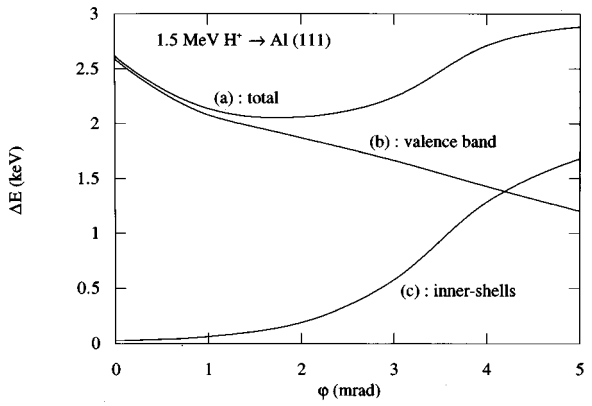

FIG. 9. Energy loss of 1.5-MeV protons specularly reflected from an aluminum (111) surface as a function of the angle of incidence. Curve *a* is the total energy loss, curve *b* is the contribution of the valence-band excitations and curve *c* is the contribution of inner-shell excitation. In the description of the valence band of the aluminum $r_s=2.07$ and $\gamma=1.35$ eV have been used.

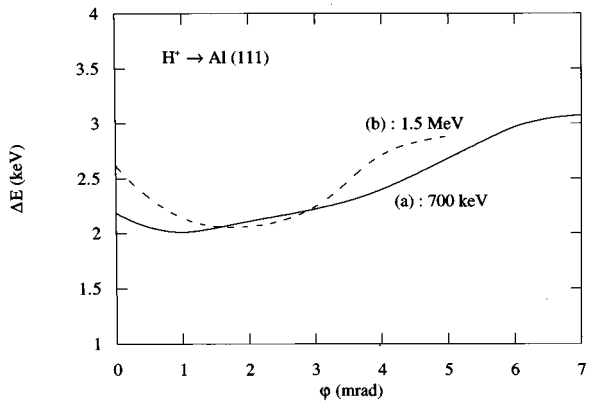

FIG. 11. Comparison of the total energy loss as a function of the angle of incidence for protons with two different initial energies incident over an aluminum (111) surface. Curve *a* corresponds to the case of 700-keV protons and curve *b* to the case of 1.5-MeV protons. The conduction band defining parameters for aluminum are $r_s=2.07$ a.u. and $\gamma=1.35$ eV.

ton travels below the electronic surface, which decreases with increasing angle of incidence.

In Fig. 10 we compare $\Delta E_{\rm val}$ calculated using the formalism described in last section to that calculated from expression (25) for 700-keV protons as a function of the angle of incidence. $dE_{\rm bulk}/dx$ is obtained using linear response theory with the RPA (Ref. 25) dielectric function and the Mermin prescription[26] and L is calculated using Eq. (19) for v_z, assuming that the solid surface is placed at a distance $d/2$ above the first atomic layer, i.e., at the jellium edge:

$$L=2v\int_{z_0}^{d/2}\frac{dz}{v_z(z)}. \tag{26}$$

The Molière potential has been used in the calculation of $v_z(z)$. As we expected, the behavior of both calculations is similar except for small angles of incidence, for which the distance of closest approach lies outside the jellium edge, and consequently, Eq. (25) gives no energy loss.

The inner-shell contribution becomes relevant only when the turning point is very close to the surface, where dE_s/dt takes appreciable values. The turning point is closer to the surface for larger angles of incidence, and therefore ΔE_s increases with increasing φ.

The sum of both contributions, i.e., the total energy loss ΔE, varies smoothly in the range 2–3 keV, when the angle of incidence varies between 0 and the maximum value for which the distance of closest approach is still outside the first layer of target atoms. (This angle is around 7 mrad for 700-keV protons and around 5 mrad for 1.5-MeV protons.)

Figure 11 compares the total energy loss ΔE as a function of φ for 700-keV and 1.5-MeV protons, which is similar in both cases. Although for the same angle of incidence the most energetic ions spend less time near the jellium edge, and consequently they lose less energy exciting the valence band (as can be observed by comparing Figs. 8 and 9), their turning point is closer to the surface, so that they lose more energy exciting inner shells. These two effects seem to almost compensate each other, and thus the total energy loss is nearly independent of the particle energy for such fast particles.

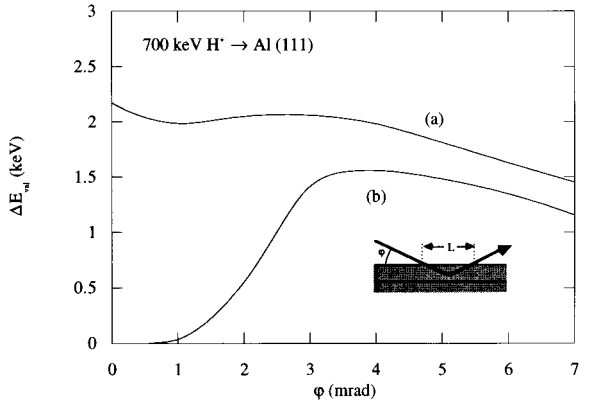

FIG. 10. Contribution of the valence-band excitation mechanism to the energy loss as a function of the angle of incidence for 700-keV protons specularly reflected at an aluminum (111) surface. Curve *a* is the result of our model and curve *b* is obtained from Eq. (25), where L is calculated using expression (26) (see also inset). The conduction band defining parameters for aluminum are $r_s=2.07$ a.u. and $\gamma=1.35$ eV.

C. Comparison with experiments

In order to compare with available experimental data[39,40] we apply our model to calculate the energy loss of protons incident over (100) surfaces of SnTe and PbSe single crystals. These materials are semiconductors with a very small gap (<0.1 eV).[41,42] This suggests that we can calculate the contribution to the energy loss of the valence band of these materials using our model for the valence-band electrons of metals. This band includes the 4 electrons of the *O* shell of Sn and the 6 electrons of the *O* shell of Te in the case of SnTe, and the 4 electrons of the *P* shell of Pb and the 6 electrons of the *N* shell of Se in the case of PbSe. In both cases, there are 5 electrons per atom in the valence band. In our model we need to determine r_s and γ. From the experi-

mental value of the bulk plasmon energy[43] (15 eV for SnTe and 15.8 eV for PbSe) we obtain effective values for the one-electron radius in these materials: $r_s=2.14$ a.u. for SnTe and $r_s=2.07$ a.u. for PbSe. The volume per atom obtained from the lattice constant of these materials compiled with the one-electron volume calculated from r_s leads to the conclusion that there are 5.06 electrons per atom in the case of SnTe and 5.24 electrons per atom in the case of PbSe effectively contributing to the valence band. These values prove that it is reasonable to approximate these electrons by free electrons. The value of the damping γ is deduced from the experimental width of the plasmon peak that is around 5 eV in both cases.[43]

Energy loss originating in the excitation of the *N* and *M* shells of Sn and Te atoms in the case of SnTe, and of the *O* and *N* shells of Pb and *M* shell of Se in the case of PbSe, are calculated using our inner-shell excitation model. The contribution of other inner-shell excitations to the stopping is negligible, and thus they are not included in the calculation. This is related to the fact that only electrons with velocities smaller than or of the order of the velocity of the projectile can be efficiently excited. In our case, the electrons that have not been included in the calculation are much faster than the incident proton.

In Fig. 12 we present results for the total energy loss as a function of the angle of incidence for 500-keV protons incident on a SnTe(100) surface, including the comparison with the experimental data and the calculation of Ref. 40. In Fig. 12(a) the results have been obtained using the Molière potential in the calculation of the trajectory and in Fig. 12(b) the ZBL potential. In these figures we also present results for the total energy loss, obtained calculating the contribution of the valence-band electrons as if they were bound atomic electrons, with the model for inner-shell electrons described in Sec. II A 2. We shall denote this model B, and the model presented in previous sections, which consists in treating the valence band using dielectric theory, will be referred to as model A from now on. No large difference is found for large incidence angles between the results of both models. For small angles of incidence, higher energy losses are obtained using model A. This is easily understood since for small angles the long-range excitation processes such as surface plasmon creation dominate. Although model A gives better quantitative agreement with the experimental data, the qualitative trend is better obtained considering the outer-shell electrons bound as bound to the target atoms. Further experimental research is required in order to determine what is the most suitable description for these electrons. It would be interesting to perform experiments with an aluminum target, for which model A is expected to be more adequate.

In Fig. 13 we present the results of our model for the energy loss induced by the inner-shell electrons compared to results obtained based on the model applied to the calculation of the energy loss induced by single-particle excitation in Refs. 39, 40. In the latter, the local density approximation is used, assuming that the stopping power is only a function of the electron density at the position of the proton. The stopping power is calculated using an expression valid for high projectile velocities in an infinite homogeneous medium,[44] in which the electrons are considered as free and the electronic density depends on z, the distance to the surface. The z-dependent electronic density is derived in some cases from the continuum surface planar potential using the Poisson equation,[39] and in other cases from the Hartree-Fock wave functions of the isolated atoms.[40] Results are presented for 500-keV protons incident on a SnTe(100) surface as a function of the angle of incidence. The continuous curve *a* stands for the results obtained by applying model B only to the inner-shell electrons and treating the valence-band electrons using the linear response theory and curve *b* shows the results obtained by applying model B to all electrons of the solid including the valence-band electrons. The dashed

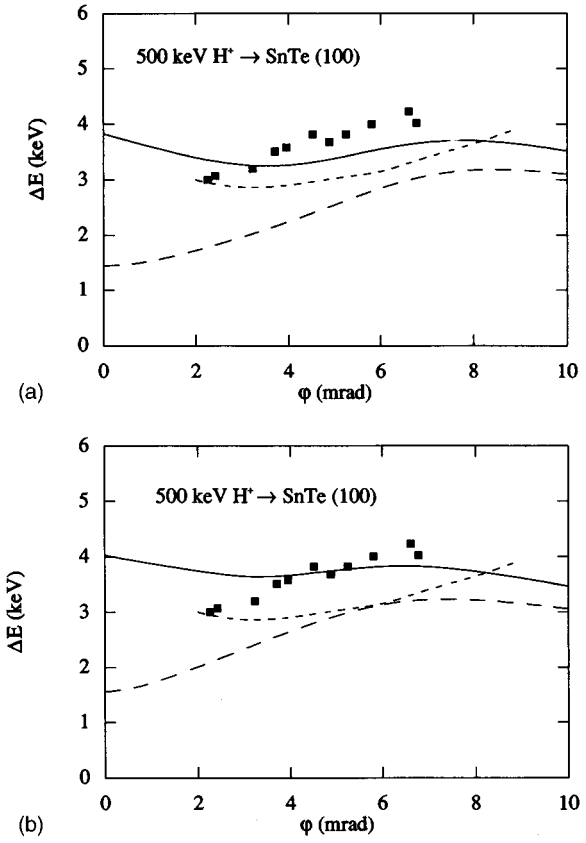

FIG. 12. (a) Energy loss as a function of the angle of incidence for 500-keV protons incident on a SnTe(100) surface. The solid line represents our model calculation, i.e., linear response theory to calculate the contribution of the valence band ($r_s=2.14$ a.u. and $\gamma=5$ eV) and localized electron model for the rest of the electrons. The dashed line shows the values obtained using our model for localized electrons for all the electrons (including the valence band electrons). The Molière potential has been used in the calculation of both curves. The square points are the experimental values taken from Ref. 40 and the dotted line the results obtained from their calculation. (They use the ZBL potential.) (b) Energy loss as a function of the angle of incidence for 500-keV protons incident on a SnTe(100) surface. The solid line represents our model calculation, i.e., linear response theory to calculate the contribution of the valence band ($r_s=2.14$ a.u. and $\gamma=5$ eV) and localized electron model for the rest of the electrons. The dashed line shows the values obtained using our model for localized electrons for all the electrons (including the valence-band electrons). The ZBL potential has been used in the calculation of both curves. The square points are the experimental values taken from Ref. 40 and the dotted line the results obtained from their calculation.

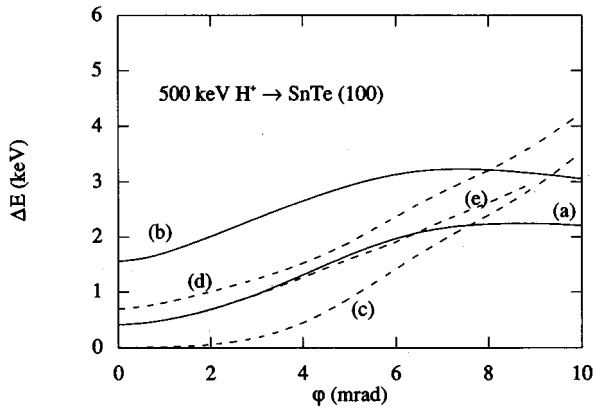

FIG. 13. Comparison between the results of the model of Refs. 39 and 40 for the energy loss induced by single-particle excitations and our model results for the energy loss produced in the excitation of inner shells as a function of the angle of incidence. Results are presented for 500-keV protons incident on a SnTe(100) surface. The ZBL potential has been used in the calculation of the trajectory. Solid curve *a* represents our results for the contribution of inner-shell electrons to the energy loss. Solid curve *b* stands for the results of our model B (see text) applied to all the electrons in the solid, including valence-band electrons. Dashed curve *c* is obtained using the model of Refs. 39 and 40 to calculate the position-dependent stopping power, where the position-dependent electronic density is derived from the Hartree-Fock wave functions of inner-shell electrons. Dashed curve *d* is the same model as in curve *c* including the electron density of the outer shell electrons calculated from the Hartree-Fock wave functions. In dashed curve *e* the same model is used and the electron density has been calculated from the planar potential using the Poisson equation. In curves *c*, *d*, and *e*, the local density approximation is used in the calculation of the position-dependent stopping power. Curves *a* and *b* include nonlocal effects.

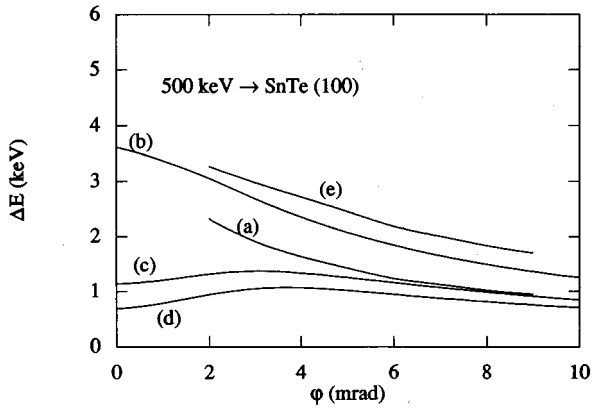

FIG. 14. Comparison between the model of Ref. 40 for collective excitations and our model for the excitations of the conduction band. Results are presented for 500-keV protons incident on a SnTe (100) surface. The ZBL potential has been used in the calculation of the trajectory. Curve *a* shows the results of Ref. 40 for the energy loss induced in the excitation of collective modes. Curve *b* is the result for the energy loss induced by the valence-band electrons within our model A (see text) (r_s=2.14 a.u., γ=5 eV). Curve *c* is the contribution of these electrons calculated using our model for localized electrons. Curve *d* is obtained using the model for single-particle excitation of Ref. 40 applied to the valence electrons, the electron density is calculated from the Hartree-Fock wave functions. Curve *e* is the sum of curves *d* and *a*.

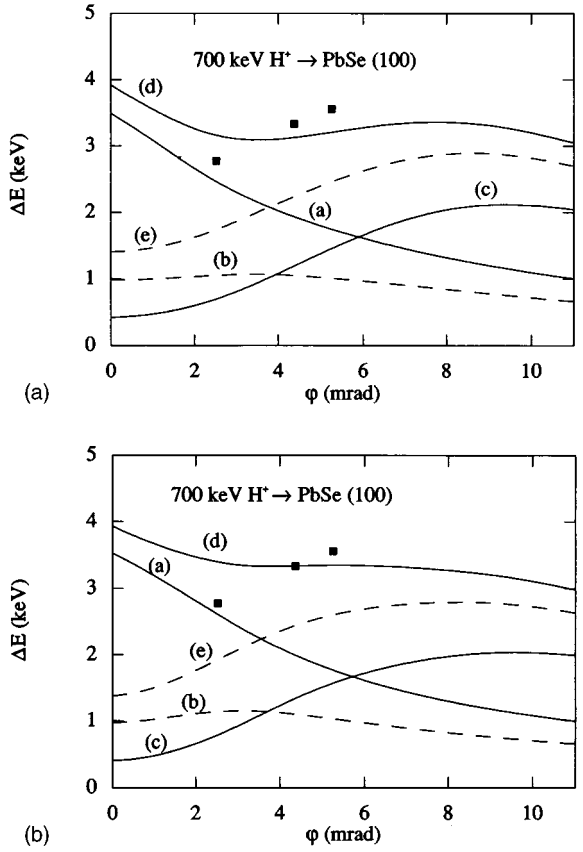

FIG. 15. (a) Energy loss of 700-keV protons specularly reflected from a PbSe (100) surface as a function of the angle of incidence. The Molière potential is used in the calculation of the trajectory. Curve *a* is the contribution of the valence band calculated using linear response theory (the free electron gas parameters used are r_s=2.07 a.u., γ=5 eV). Dashed curve *b* is this contribution calculated using the model for localized electrons. Curve *c* shows our model results for inner-shell electrons. Curve *d* is the sum of curve *a* and curve *c*, the total energy loss when the valence electrons are considered free. Dashed curve *e* is the sum of curves *b* and *c*, the total energy loss when all the electrons are considered bound to the target atoms. The square points are experimental data from Ref. 39. (b) Energy loss of 700-keV protons specularly reflected from a PbSe(100) surface as a function of the angle of incidence. The ZBL potential is used in the calculation of the trajectory. Curve *a* is the contribution of the valence band calculated using linear response theory (the free electron gas parameters used are r_s=2.07 a.u., γ=5 eV). Dashed curve *b* is this contribution calculated using the model for localized electrons. Curve *c* shows our model results for inner-shell electrons. Curve *d* is the sum of curve *a* and curve *c*, the total energy loss when the valence electrons are considered free. Dashed curve *e* is the sum of curves *b* and *c*, the total energy loss when all the electrons are considered bound to the target atoms. The square points are experimental data from Ref. 39.

curves *c*, *d*, and *e* correspond to values obtained using the model of Refs. 39 and 40 for single-particle excitations. The distance-dependent electron density is calculated from the Hartree-Fock wave functions of the inner-shell electrons in curve *c*, from the Hartree-Fock wave functions of all electrons (including valence-band electrons) in curve *d* and from the continuum surface potential using the Poisson equation in curve *e*. Comparison between curves *a* and *c*, and be-

tween curves *b* and *d* shows that the local density approximation underestimates the energy loss for small angles, for which large impact parameters are involved and the proton passes through the low-density region. On the other hand, for larger angles, for which the proton goes through higher density regions, it overestimates the energy loss.

In Fig. 14 a comparison between different approximations for the energy loss due to the excitation of the valence band of the metal is presented. Results for 500-keV protons incident on a SnTe(100) surface are presented as a function of the angle of incidence. Curve *a* corresponds to the results of Ref. 40 for the energy loss induced by collective excitations. In this calculation, a formula for an inhomogeneous electron gas derived by Kitagawa[45] in the high-frequency approximation has been used. The distance-dependent valence-electron density is approximated by the electronic density calculated from the atomic wave functions in the Hartree-Fock approximation. Results obtained for the valence-band-induced energy loss using our model A (curve *b*) and our atomic model B (curve *c*) are also presented. A large difference between curves *b* and *c* is observed at small angles, for which plasmon excitation is an important contribution in model A. In curve *d* we plot the values obtained using the model of Refs. 39 and 40 for single-particle excitations applied to the valence-band electrons. Curve *e* shows the sum of curves *a* and *d*. It can be understood as the total energy loss induced by the valence band within the model of Refs. 39 and 40. Results of curve *e* and our model A results show the same qualitative behavior of the energy loss in its dependence with the angle of incidence, though our model predicts a slightly lower energy loss.

Finally, Fig. 15 illustrates the results for the total energy loss as a function of the angle of incidence for 700 keV on a PbSe(100) surface, including the comparison with available experimental data.[39] The trajectories have been calculated using the Molière potential in Fig. 15(a) and the ZBL potential in Fig. 15(b). Two different models have been used to describe the outer-shell electrons. Solid curve *a* is the contribution of these electrons to the energy loss when the linear response theory is used (model A), and dashed curve *b* when they are considered as bound to the target atoms and our model B is used. Curve *c* is the contribution of the inner-shell electrons. Curve *e* is the sum of curve *c* and curve *b*, i.e., the total energy loss when all electrons are considered to be localized. Curve *d* is the sum of curves *a* and *c*, the total energy loss when linear response theory is applied to calculate the valence-band contribution. Better quantitative agreement is achieved, as above, using model A for outer-shell electrons, but again the qualitative trend is better obtained when all electrons are considered localized.

IV. SUMMARY

We have developed a parameter-free theoretical calculation of the energy loss of fast protons under grazing incidence over a metal surface. The losses due to excitation of both inner-shell electrons of target atoms and the valence band are considered separately. The former is obtained from a first Born approximation calculation, while the latter is derived from the induced surface wake concept. The results show that the energy loss remains practically constant when the angle of incidence is changed and that it is almost independent of the initial energy of the projectiles. The comparison with available experiments on semiconductors shows a good overall agreement. However, it is not completely clear whether it is better to replace the valence-band electron model by localized target atom electron states. It would be very interesting to perform experiments on metallic aluminum for which the valence electron model is expected to be more adequate.

ACKNOWLEDGMENTS

The authors want to express their gratitude to A. Salin for providing them with the programs to calculate the contribution of inner-shell electrons. They also acknowledge help and support by the Departamento de Educación del Gobierno Vasco, the Diputación Foral de Gipuzkoa and the Spanish Ministerio de Educación y Ciencia.

[1] A. Närmann, R. Monreal, P. M. Echenique, F. Flores, W. Heiland, and S. Schubert, Phys. Rev Lett. **64**, 1601 (1990).
[2] A. Närmann, W. Heiland, R. Monreal, F. Flores, and P. M. Echenique, Phys. Rev B **44**, 2003 (1992).
[3] A. Närmann, H. Franke, K. Schmidt, A. Arnau, and W. Heiland, Nucl. Instrum. Methods B **69**, 158 (1992).
[4] A. Närmann, K. Schmidt, C. Höfner, W. Heiland, and A. Arnau, Nucl. Instrum. Methods B **78**, 72 (1992).
[5] M. Wilke, R. Zimny, and H. Winter, Nucl. Instrum. Methods B **100**, 396 (1995).
[6] F. Stölzle and R. Pfandzelter, Europhys. Lett. **20**, 369 (1992).
[7] R. Pfandzelter and F. Stölzle, Nucl. Instrum. Methods B **72**, 163 (1992).
[8] H. D. Hagstrum, Phys. Rev. **96**, 336 (1954).
[9] R. Zimny, Z. L. Miskovic, N. N. Nedeljkovic, and Lj. D. Nedeljkovic, Surf. Sci. **255**, 135 (1991).
[10] N. Lorente, R. Monreal, and M. Alducin, Phys. Rev. A **49**, 4716 (1994).
[11] Y. Fujii, K. Narumi, K. Kishine, K. Kimura, and M. Mannami, Nucl. Instrum. Methods B **67**, 82 (1992).
[12] K. Narumi, Y. Fujii, K. Kishine, H. Kurakake, K. Kimura, and M. Mannami, Surf. Sci. **293**, 152 (1993).
[13] J. I. Juaristi and F. J. García de Abajo, Nucl. Instrum Methods B **90**, 252 (1994).
[14] Y. Fujii, K. Kishine, K. Narumi, K. Kimura, and M. Mannami, Phys. Rev. A **47**, 2047 (1993).
[15] R. H. Ritchie, Phys. Rev. **106**, 874 (1957).
[16] P. M. Echenique and J. B. Pendry, J. Phys. C **8**, 2936 (1975).
[17] R. H. Ritchie and A. L. Marusak, Surf. Sci. **4**, 234 (1966).
[18] D. Wagner, Z. Naturforsch A **21**, 634 (1966).
[19] J. Heinrichs, Phys. Rev. B **8**, 1346 (1973).
[20] F. Flores and F. García Moliner, J. Phys. C **12**, 907 (1979).
[21] R. Nuñez, P. M. Echenique, and R. H. Ritchie, J. Phys. C **13**, 4229 (1980).
[22] N. Zabala and P. M. Echenique, Ultramicroscopy **32**, 327 (1990).
[23] F. J. García de Abajo and P. M. Echenique, Phys. Rev. B **46**, 2663 (1992).

[24] F. J. García de Abajo and P. M. Echenique, Phys. Rev. B **48**, 13 399 (1993).
[25] J. Lindhard, K. Dans. Vidensk. Selsk. Mat. Fys. Medd **28** (8) (1954).
[26] N. D. Mermin, Phys. Rev. B **1**, 2362 (1970).
[27] J. M. Cowley, Surf. Sci. **114**, 587 (1992).
[28] A. Howie and R. H. Milne, Ultramicroscopy **18**, 425 (1985).
[29] M. R. C. Mcdowell and J. P. Coleman, *Introduction to the Theory of Ion-Atom Collisions* (North-Holland, Amsterdam, 1970).
[30] R. McCarroll and A. Salin, C. R. Acad. Sci. Paris B **263**, 329 (1966).
[31] J. P. Desclaux, Comput. Phys. Commun. **1**, 216 (1969).
[32] A. Salin, J. Phys. B **22**, 3901 (1979).
[33] H. Winter, Phys. Rev. A **46**, R13 (1992); Europhys. Lett. **18**, 107 (1992).
[34] V. G. Molière, Z. Naturforsch. A **2**, 133 (1947).
[35] J. F. Ziegler, J. P. Biersack, and U. Littmark, *The Stopping and Range of Ions in Matter*, edited by J. F. Ziegler (Pergamon, New York, 1985), Vol. 1.
[36] J. P. Muscat and D. M. Newns, Surf. Sci. **64**, 641 (1977).
[37] P. M. Echenique, F. J. García de Abajo, V. H. Ponce, and M. E. Uranga, Nucl. Instrum. Methods B **96**, 583 (1995).
[38] P. M. Echenique, F. Flores, and R. H. Ritchie, in *Solid State Physics: Advances in Research and Applications*, edited by H. Ehrenreich and D. Turnbull (Academic, New York, 1990), Vol. 43, p. 229.
[39] Y. Fujii, S. Fujiwara, K. Narumi, K. Kimura, and M. Mannami, Surf. Sci. **277**, 164 (1992).
[40] K. Kimura, H. Kuroda, M. Fritz, and M. Mannami, Nucl. Instrum. Methods B **100**, 356 (1995).
[41] M. Cardona and D. L. Greenaway, Phys. Rev. **133**, A1685 (1964).
[42] P. J. Lin and L. Kleinman, Phys. Rev. **142**, 478 (1966).
[43] B. Lahaye, F. Pradal and C. Gout, J. Phys. (Paris) **29**, C4-137 (1968).
[44] J. J. Thompson, Philos. Mag. **23**, 419 (1912).
[45] M. Kitagawa, Nucl. Instrum. Methods B **33**, 409 (1988).